nature geoscience

Article

https://doi.org/10.1038/s41561-023-01227-x

A seasonally ice-free Arctic Ocean during the Last Interglacial

Received: 17 June 2022

Accepted: 22 June 2023

Published online: 3 August 2023

Check for updates

Flor Vermassen[1,2] ✉, Matt O'Regan[1,2], Agatha de Boer[1,2], Frederik Schenk[1,2], Mohammad Razmjooei[1,2], Gabriel West[1,2], Thomas M. Cronin[3], Martin Jakobsson[1,2] & Helen K. Coxall[1,2]

The extent and seasonality of Arctic sea ice during the Last Interglacial (129,000 to 115,000 years before present) is poorly known. Sediment-based reconstructions have suggested extensive ice cover in summer, while climate model outputs indicate year-round conditions in the Arctic Ocean ranging from ice free to fully ice covered. Here we use microfossil records from across the central Arctic Ocean to show that sea-ice extent was substantially reduced and summers were probably ice free. The evidence comes from high abundances of the subpolar planktic foraminifera *Turborotalita quinqueloba* in five newly analysed cores. The northern occurrence of this species is incompatible with perennial sea ice, which would be associated with a thick, low-salinity surface water. Instead, *T. quinqueloba*'s ecological preference implies largely ice-free surface waters with seasonally elevated levels of primary productivity. In the modern ocean, this species thrives in the Fram Strait–Barents Sea 'Arctic–Atlantic gateway' region, implying that the necessary Atlantic Ocean-sourced water masses shoaled towards the surface during the Last Interglacial. This process reflects the ongoing Atlantification of the Arctic Ocean, currently restricted to the Eurasian Basin. Our results establish the Last Interglacial as a prime analogue for studying a seasonally ice-free Arctic Ocean, expected to occur this century.

Arctic sea ice plays an important role in the climate system. It insulates the ocean from heat loss and largely determines the Arctic surface albedo[1]. Modern sea-ice cover is reducing rapidly, and most simulations predict at least one ice-free month in summer before the year 2050[2]. A changing sea-ice cover can trigger positive feedback processes that influence regional and global climate, which need to be well understood. Identifying the last time Arctic sea ice disappeared is therefore important for anticipating future changes as well as providing targets for testing climate model performance[3]. The Last Interglacial (LIG; the Eemian, Marine Isotope Stage 5e (MIS5e) ~129–115 thousand years before present (ka BP)) is a particularly well-suited period to study ongoing Arctic sea-ice change as terrestrial circum-Arctic summer temperatures were ~4–5 °C degrees warmer than today[4], and boreal forests extended to the Arctic Ocean coastline[5]. However, the extent of Arctic sea ice during this time is debated and hinders a comprehensive understanding of the LIG climate. So far, climate models and proxy records have mostly suggested a relatively extensive perennial sea-ice cover[6,7], although some studies have hinted at a more reduced ice pack or a seasonally ice-free Arctic Ocean[8–10]. The uncertainty in sea-ice reconstructions is due in part to limited proxy-record coverage across the Arctic Ocean. In particular, there has been a dearth of records from the difficult-to-reach central Arctic Ocean, where the thickest sea ice persists. In this Article, we investigate sediment cores from this key area and other parts of the Arctic Ocean, using distribution patterns

[1]Department of Geological Sciences, Stockholm University, Stockholm, Sweden. [2]Bolin Centre for Climate Research, Stockholm University, Stockholm, Sweden. [3]Florence Bascom Geoscience Center, US Geological Survey, Reston, VA, USA. ✉e-mail: flor.vermassen@geo.su.se

https://doi.org/10.1038/s41561-023-01227-x

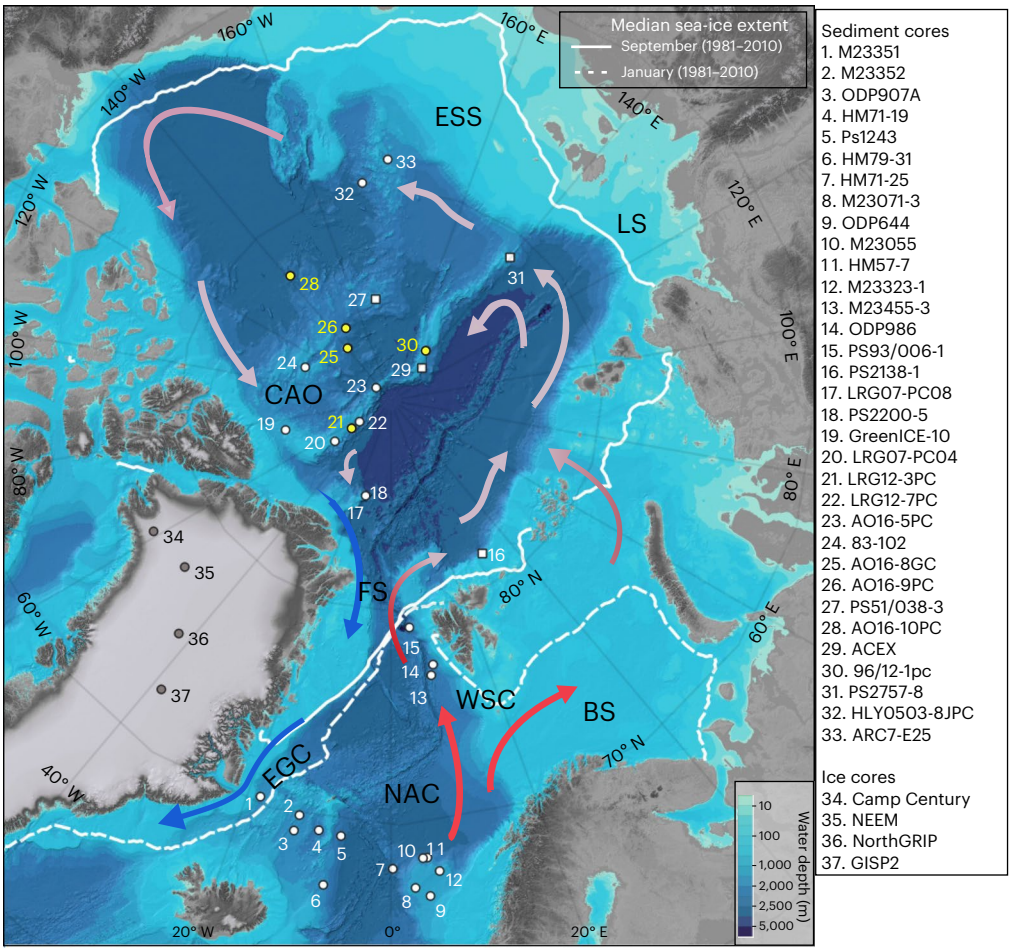

Fig. 1 | Study area and core sites. Overview of marine sediment cores and ice cores mentioned in the text, together with the bathymetric map of the Arctic Ocean[53] and mean ice-edge positions during September and January for the period 1981–2010[54]. Yellow circles indicate core sites with new microfossil data. White circles indicate sites with microfossil data that is used in the data compilation (Extended Data Table 1). White squares indicate sites used for comparison with stratigraphic and geochemical data, these sites either have no planktic assemblage data from the >63 µm fraction (sites 16, 27) or calcareous microfossils are not well preserved (sites 29, 31). Grey circles are ice-core sites. The modern pathway of Atlantic-derived ocean currents is indicated with red arrows; the colour transparency change signifies subduction of Atlantic Waters beneath the 100–200-m-thick Arctic halocline. NAC, Norwegian Atlantic Current; WSC, West Spitsbergen Current; EGC, East Greenland Current; CAO, Central Arctic Ocean; FS, Fram Strait; BS, Barents Sea; ESS, East Siberian Sea; LS, Laptev Sea. The ice edge is defined as locations with a 50% probability of ice occurring at a concentration of 15% or greater[54]. Figure adapted from ref. 1 under a Creative Commons license CC BY 4.0.

of the classic subpolar foraminifera species *Turborotalita quinqueloba* to demonstrate seasonally ice-free conditions during the LIG.

The ecology and role of *T. quinqueloba*

At high northern latitudes, the planktic foraminifer *T. quinqueloba* (genetic type IIa[11]) is considered a subpolar species thriving in areas that are largely ice free or bordering the sea-ice edge, predominantly in the Arctic–Atlantic gateways of the Barents Sea and Fram Strait[12–17]. A key observation is that *T. quinqueloba* abundance coincides with incoming Atlantic waters, while the East Greenland Current, composed of cold, low-salinity surface waters exiting the Arctic, contains very few *T. quinqueloba*[15] (Extended Data Figs. 1 and 2). By contrast, the Arctic specialist *Neogloboquadrina pachyderma* (genetic type I[11]) has a much broader distribution, tolerating the polar extremes of the central Arctic Ocean, even under perennial sea ice, and occurs throughout the Nordic Seas and Fram Strait–Barents Sea region, including the East Greenland Current (Extended Data Figs. 1 and 2)[15–18]. A clear ecological boundary occurs northwest of Svalbard, at the border of the central Arctic Ocean province, beyond which resident populations of *T. quinqueloba* do not occur today and where *N. pachyderma* dominates (Extended Data Fig. 3)[17,18]. This boundary coincides with Atlantic Water sinking to depths of 200–500 m below the 100–200-m-thick Arctic halocline, in turn capped by the cold and fresh polar mixed layer[19] (5–50 m thick; Fig. 1 and Extended Data Fig. 4). Rare living *T. quinqueloba* have been found at latitudes up to 86° N, but such individuals are considered advected non-residents, their main habitat and reproducing area occurring southwards[18]. Presumably, *T. quinqueloba* disappears in the central Arctic either because its preferred Atlantic Water habitat and associated food source is no longer at the surface, and/or it cannot tolerate the cold, fresh polar mixed layer and extensive sea-ice cover.

On the basis of the preceding associations, *T. quinqueloba* is often considered a reliable proxy for Atlantic Water influence in the sub-Arctic North Atlantic and has been used for reconstructing the position of the sea-ice edge, the Arctic front[20,21] and even the extent of Arctic Atlantification in the Fram Strait[22]. Preferences for particular temperature and salinity conditions have been shown in a broad sense; for example, in the Fram Strait, *T. quinqueloba* occurs in temperatures of 0.7–3.4 °C and salinities of 34–35 psu (ref. 17). In the North Atlantic, peak abundances occur broadly at water temperatures of 4–7 °C and salinities of 34.8–35.1 psu (ref. 23), supporting a general intolerance

https://doi.org/10.1038/s41561-023-01227-x

of low-salinity polar surface waters (Extended Data Figs. 1, 2 and 5). Importantly, living *T. quinqueloba* abundance in the water column shows a predictable seasonal pattern, with one to two peaks per year, demonstrating that *T. quinqueloba* occurrence is also strongly coupled to the primary productivity cycle, in addition to temperature and salinity regimes[12,14,15,24]. The abundance of *N. pachyderma* also shows a seasonal signal, as observed in the Nordic Seas[24]. However, it appears to have greater potential to overwinter beneath sea ice, perhaps having evolved a stage of reduced metabolism or ability to harvest ice-stored organic matter that *T. quinqueloba* lacks[14].

Invasion of the Arctic Ocean by *T. quinqueloba*

Our new planktic foraminifer assemblage records from five sites across the central Arctic Ocean (AO16-10PC, AO16-9PC, AO16-8GC, LRG12-3PC, 96/12-1pc) show that *T. quinqueloba* is largely absent from the modern central Arctic Ocean, in agreement with previous research[25] (only rare individuals were found in near-surface sediments of core AO16-10PC). By contrast, sediment intervals dated to MIS5 (MIS5a to MIS5e) consistently record multiple abundance peaks of *T. quinqueloba* that account for 30–60% of the planktic foraminifera assemblage (Fig. 2). The age resolution of the MIS5 interval is ~2,000 yr cm^{-1} in all five records. We compile these results with all previously reported *T. quinqueloba* LIG occurrences from the Arctic and northern North Atlantic (Fig. 3 and Extended Data Table 1). Age models for the new cores rely on lithostratigraphic correlation to dated sedimentary sequences on the Lomonosov Ridge, in particular to the classic sediment cores LRG12-3PC, ACEX and 96/12-1pc[26–28] (Extended Data Fig. 6). We show that in all central Arctic cores where calcareous microfossils are well preserved, *T. quinqueloba* occurs throughout the entire MIS5 interval, in conjunction with *N. pachyderma* (Figs. 2 and 3 and Extended Data Fig. 9). At the base of the MIS5 interval, interpreted to represent MIS5e, the *T. quinqueloba* abundance is generally highest and most consistent, reaching up to 60% of foraminifera assemblages. In all cores, *T. quinqueloba* abundances are low in the mid part of the MIS5 interval (MIS5b–5d), where *N. pachyderma* dominance returns. At the top of the MIS5 interval (MIS5a), *T. quinqueloba* abundance increases again in some cores (Fig. 2). Extremely rare occurrences (1–2 individuals) of another subpolar species, *Globigerinita uvula*, also occur in cores AO16-8GC (MIS5e) and LRG12-3PC (MIS5e and 5a). Neither *Neogloboquadrina incompta* nor *Globigerina bulloides* was observed; nor were other species.

Interpreting Arctic Ocean ice conditions and oceanography

The *T. quinqueloba* invasion documents a remarkable transformation of the central Arctic Ocean to subpolar-type conditions during the LIG. Extending the *T. quinqueloba* ecological constraints back in time, we propose that oceanic conditions comparable to those currently found in the Fram Strait/Barents Sea had propagated into the central Arctic Ocean. This implies that vast areas of open water and immensely reduced summer sea ice characterized the central Arctic Ocean. These conditions allowed seasonal primary production maxima supporting prolific *T. quinqueloba* populations. The spatial distribution of sediment cores with maximal *T. quinqueloba* abundances allows us to delineate a boundary of the summer sea-ice minimum during the LIG. Under the assumption that sea-ice retreat during the LIG occurred in a manner similar to the pattern of modern ice retreat, sea ice could not have extended farther than ~500 km from the Greenland–Canada coast (Fig. 3). Modern observations and model projections indeed identify the coastal zones bordering Canada–Greenland as the 'last ice area' for retreating sea ice, as a result of the configuration of Arctic winds and currents[29]. Moreover, simulations of sea ice also showed that the spatial pattern of sea-ice retreat during the LIG largely mimicked that of modern sea-ice retreat[7]. The northward expansion of boreal forest right up to the Arctic coastline with reconstructed temperatures 9 °C higher than today, as documented in Western Beringia[5], also makes the persistence of multi-year sea ice in this region highly unlikely. Ice-free conditions were also proposed near Alaska on the basis of the finding of extralimital (non-native) molluscs[10]. Even if some sea ice just north of Canada/Greenland survived the summer melt, the LIG summer sea-ice

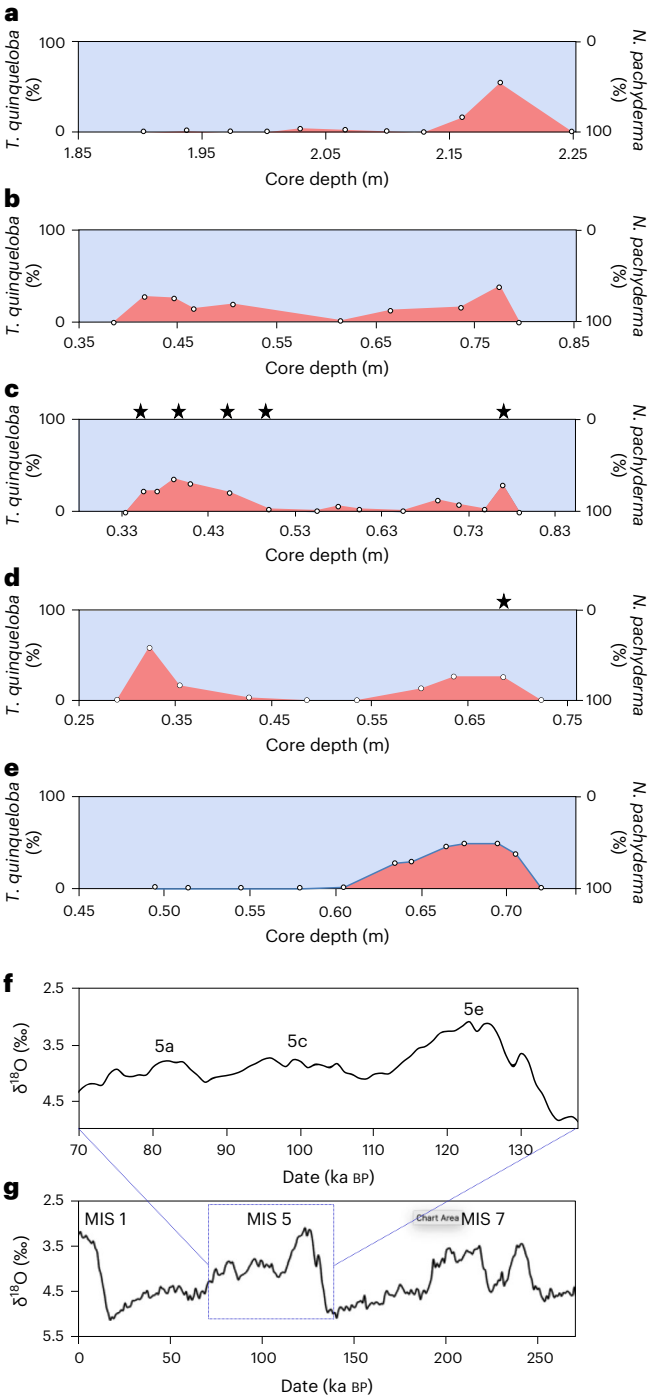

Fig. 2 | Foraminiferal data. a–f, Downcore variation of planktic foraminifera assemblage composition in the MIS5 interval in the central Arctic Ocean from key cores 96/12-1pc (**a**), AO16-9PC (**b**), LRG12-3PC (**c**), AO16-8GC (**d**) and AO16-10PC (**e**). Red colours indicate *T. quinqueloba* abundance; blue colours indicate *N. pachyderma* abundance. Star symbols indicate very rare occurrences of *Globigerinita uvula*. For stratigraphic context, see Extended Data Fig. 6. **f**, Global benthic δ^{18}O stack for MIS5[55], with marine isotope substages indicated. **g**, Global benthic δ^{18}O stack for the past 270 kyr.

https://doi.org/10.1038/s41561-023-01227-x

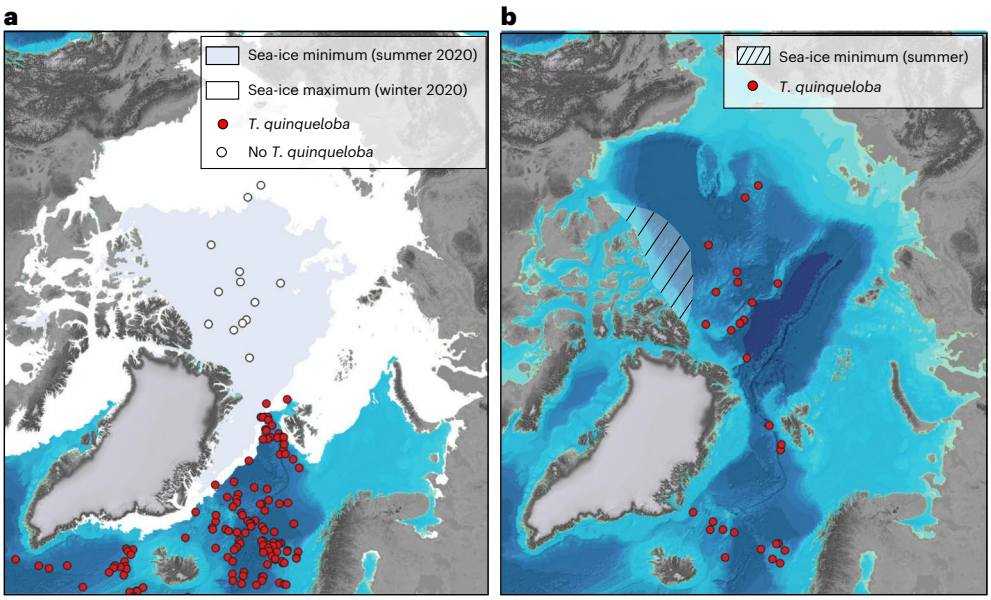

Fig. 3 | Data compilation and interpretation. Compilation of new and existing *T. quinqueloba* occurrences (>1% of the seafloor assemblage) during modern times and the LIG, together with observed and reconstructed sea-ice conditions, with bathymetric map in the background[53]. **a**, Modern *T. quinqueloba* occurrences and sea-ice cover. Data are from published databases[56,57] combined with results from this study. Sea-ice extent from 2020 is from NSIDC[58]. **b**, *T. quinqueloba* occurrences and sea-ice cover during the LIG. The extent of the LIG summer minimum sea-ice extent is inferred on the basis of our new *T. quinqueloba* constraints, assuming this species requires largely ice-free summers. This is a maximal estimate for the summer sea-ice minimum since there are currently no observations (sediment cores) north of the Canadian Arctic Archipelago region that comprise LIG sediments (shown by the diagonal hatched region)[59–70]. Figure adapted from ref. 53 under a Creative Commons license CC BY 4.0.

minimum area could not have constituted more than 600,000 km^2, which is well below the 1,000,000 km^2 limit used as a threshold for an ice-free Arctic Ocean (hatched area in Fig. 3). The uncertainty about ice persisting in the region just north of Canada/Greenland exists because it remains a major gap for sediment coring and proxy data, implying that our reconstruction represents a maximal estimate of the extent of the sea-ice minimum. Since *T. quinqueloba* populations are highly seasonal[24] and *N. pachyderma* remained present during the LIG, relatively extensive winter ice could have persisted. In the absence of any specific proxy for winter sea-ice extent, we do not attempt to delineate the winter margin for the LIG. The Laptev and East Siberian Sea shelf regions lack constraints due to the poor quality of calcareous microfossil preservation there, a consequence of carbonate-corrosive waters derived from Siberian river discharge[30,31].

Multiple processes could lead to environmental conditions allowing *T. quinqueloba* to occupy the central Arctic Ocean. For this to happen, a stratification change involving shoaling of the halocline and/or its erosion would be required. Since *T. quinqueloba* prefers near-surface waters with Atlantic Water-influenced salinities and open waters in the summer to sustain a seasonal phytoplankton-based diet, we suggest that the Atlantic layer in the central Arctic Ocean shoaled to a water depth of ~50 m. This resulted in the northward propagation of the *T. quinqueloba* habitat, allowing it to invade the central Arctic (Fig. 4). Currently, in the southern Barents Sea, ongoing shoaling of the Atlantic Water and weakened stratification are indeed observed, and these are considered key processes contributing to the 'Atlantification' of the Arctic Ocean[32]. In the northern Barents Sea, a decrease in sea ice was shown to result in a weakened ocean stratification and increased upward fluxes of heat and salt[33], similar to observations in the Eurasian basin[34]. A class of simple conceptional models suggests that the depth of the Arctic halocline is mobile and highly dependent on freshwater perturbations where an increased freshwater input in a silled basin such as the Arctic Ocean induces a shallowing of the halocline[35]. This implies that the freshwater input from melting of surrounding continental ice sheets during the LIG may have triggered a shallowing of the halocline, allowing Atlantic Waters to reach the productive photic zone and creating the environmental conditions suited for *T. quinqueloba*. Since the Greenland Ice Sheet was strongly reduced during at least one or multiple interglacials[36,37], the prerequisite for such a scenario might well have been in place during the LIG. Another mechanism that could invoke the required stratification change is the erosion of the halocline, induced by a temperature increase of the inflowing Atlantic Water. A first-order approximation based on modern observations suggests that, given a fixed salinity of about 35 psu, an increase of the Atlantic layer temperature to about 6–7 °C would be needed to reach the same density as the bottom of the halocline and thus be conducive to mixing (Extended Data Fig. 8). Interestingly, peak occurrences of *T. quinqueloba* in the modern ocean are found exactly at these environmental conditions (Extended Data Fig. 5). However, this assumes that the halocline temperature at the LIG is similar to its modern value.

Once the optimal environmental conditions were in place, *T. quinqueloba* could theoretically have entered the Arctic Ocean from either the North Atlantic or the Pacific Ocean. Modern observations show that planktic foraminifera are not resident in, and do not migrate through, the Bering Strait, possibly because it is too shallow (sill depth ~53 m) and too acidic to support the calcifying plankton communities[38], making the Atlantic–Arctic corridor the most logical route for the subpolar invaders. Interestingly, our LIG oceanographic reconstruction appears to reflect conditions similar to those expected to develop in response to ongoing Atlantification of the Arctic[22]. For example, once sea-ice export through the Fram Strait ceases (around the year 2050), it is expected that the Arctic planktic communities in the Fram Strait will abruptly shift towards non-sea ice and Atlantic species, and that these changes will propagate into the central Arctic[12]. Since *T. quinqueloba* percentages remain high in the top of the MIS5 interval, this would suggest that similar conditions also persisted through MIS5a, which appears consistent with prolonged interglacial warmth reconstructed from lake proxy data in northern Finland[39].

https://doi.org/10.1038/s41561-023-01227-x

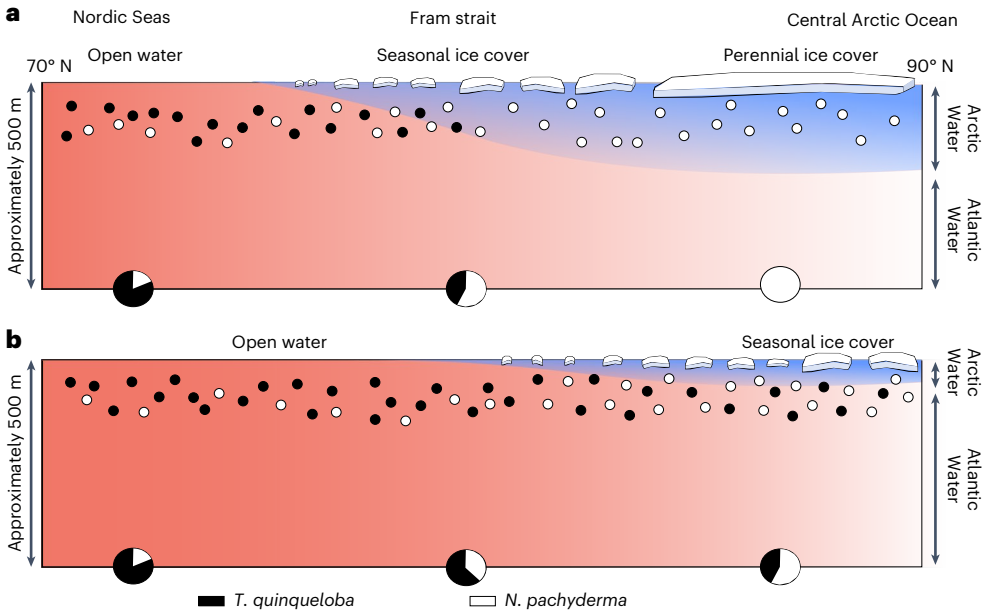

Fig. 4 | Conceptual cartoon. Illustrative model depicting ocean stratification and sea-ice conditions (upper 500 m) in the modern Nordic Seas–Arctic Ocean region (**a**) and their hypothesized transformation during the LIG (**b**). The transect is located along the 5° E meridian, from 70° N to the North Pole. The occurrences of *T. quinqueloba* and *N. pachyderma* in the water column (determined from plankton tows in the modern case, inferred from sediments for the LIG case) are indicated with small black and white circles, respectively. Their relative abundances at the seafloor (summarized from existing and new data presented here) are indicated by pie charts.

Wider perspectives on LIG sea-ice conditions and climate

Previously, the Arctic occurrence of *T. quinqueloba* and its relation to reduced sea-ice conditions during the LIG had been suggested on the basis of a single core site just north of Greenland[8]. This interpretation was later challenged, with the suggestion that there was no extensive sea-ice loss but that open-water conditions were restricted in the form of local polynyas[6]. However, there is to our knowledge no evidence of *T. quinqueloba* being associated with polynya habitats in the Arctic[40]. The invasion of the Arctic basin by *T. quinqueloba* demonstrated in this study clearly renders the polynya hypothesis unlikely and corroborates basin-wide reduced sea-ice concentrations. This finding contrasts with the extensive, perennial sea-ice-cover reconstructions based on the absence of the open-water indicator brassicasterol and low concentrations of the biomarker IP_{25} (ref. 6) (Extended Data Fig. 7). We would argue that the presence of microfossils in the sedimentary record is currently a more robust proxy that is less ambiguous to interpret compared with the absence of biomolecules since the sources and sedimentary fate of the latter are still relatively unknown and under investigation[41]. In particular, the absence of IP_{25} remains difficult to interpret since this could be due to either perennial or ice-free conditions, or may be the result of low diatom production or degradational processes, especially in offshore deep-water settings as investigated here[42]. By contrast, modern environmental conditions of subpolar foraminifera are readily observable.

Our findings substantiate several studies that have hinted at reduced ice conditions but lacked conclusive, direct evidence. On land, extralimital molluscs were found at almost every LIG locality along the Alaska coast[10]. From this, it was suggested that winter sea ice did not expand south of Bering Strait, that the Bering Sea was annually ice free and that the Arctic Ocean ice cover was perhaps only seasonal at the time[10]. In addition, a well-known feature in multiple ice-core records from Greenland (NEEM, NGRIP, GIPS2 and Camp Century) is that stable oxygen isotope values from the LIG are at least 2.5‰ higher compared with present day, implying surface air temperatures that are 8 ± 4 °C warmer than during the last millenium[43]. Climate simulations that respond solely to greenhouse gases and orbital forcing have failed to capture these $\delta^{18}O$ and temperature anomalies[4,44]. However, a recent isotope-enabled climate modelling study demonstrated that sea-ice loss was capable of producing the magnitude of the $\delta^{18}O$ anomaly[43].

Unifying this proxy-based evidence for a seasonally ice-free ocean with sea-ice reconstructions from climate models remains difficult due to the high levels of uncertainty involved in sea-ice simulations. Climate models produce LIG sea-ice conditions that range widely; most models simulate a relatively extensive, perennial sea-ice cover, whereas some simulate very little ice or ice-free conditions[7,9]. This wide spread can be expected since many general circulation models even have difficulty accurately capturing the recent changes in Arctic sea ice that have occurred during the past decades[45,46], not to mention the subtleties of ocean stratification changes. Regardless, an ice-free Arctic Ocean is much more compatible with the marked Arctic warming that occurred during the LIG than is an Arctic Ocean with an extensive, perennial ice cover[4,47]. Data compilations indeed show that high-latitude sea surface and air temperatures were warmer than present during the LIG, with global sea level estimated at 5–10 m higher than today[48–50]. Furthermore, an ice-free Arctic can provide the missing link for the longstanding puzzle of why climate models have underestimated sea and air temperatures during this period[9]. This is supported by sensitivity experiments that demonstrate a strong response of Arctic temperatures to sea-ice retreat[51]. It is further consistent with the simulation of the Hadley Centre Global Environment Model version 3, which produced an excellent match to summer Arctic temperature proxies while simulating a seasonally ice-free Arctic Ocean[9]. In addition, while modern Atlantification is currently restricted to the eastern Eurasian basin and model outputs diverge with regard to future stratification changes[52], our results demonstrate the potential for panarctic Atlantification occurring in a world of 0.5–1.5 °C above Preindustrial.

In the context of rapidly decreasing sea ice, an important goal of palaeoclimate studies is to identify the last time the Arctic became ice free. The invasion of the Arctic basin by *T. quinqueloba* provides

the first firm evidence for extensive seasonally ice-free conditions across the interior Arctic Ocean where perennial sea ice remains in place today. Therefore, we put the LIG forward as the youngest and perhaps most relevant geological period for studying a seasonally ice-free Arctic Ocean, which is expected to occur this century. This information provides a useful constraint that can be included in ocean and climate models, leading to an improved understanding of Arctic sea ice in the climate system.

Online content

Any methods, additional references, Nature Portfolio reporting summaries, source data, extended data, supplementary information, acknowledgements, peer review information; details of author contributions and competing interests; and statements of data and code availability are available at https://doi.org/10.1038/s41561-023-01227-x.

References

1. IPCC *Climate Change 2014: Synthesis Report* (eds Core Writing Team, Pachauri, R. K. & Meyer L. A.) (IPCC, 2014).
2. Notz, D., SIMIP Community Arctic sea ice in CMIP6. *Geophys. Res. Lett.* **47**, e2019GL086749 (2020).
3. Polyak, L. et al. History of sea ice in the Arctic. *Quat. Sci. Rev.* **29**, 1757–1778 (2010).
4. Otto-Bliesner, B. L. et al. How warm was the Last Interglacial? New model–data comparisons. *Phil. Trans. R. Soc. A* **371**, 20130097 (2013).
5. Kienast, F. et al. Paleontological records indicate the occurrence of open woodlands in a dry inland climate at the present-day Arctic coast in western Beringia during the Last Interglacial. *Quat. Sci. Rev.* **30**, 2134–2159 (2011).
6. Stein, R., Fahl, K., Gierz, P., Niessen, F. & Lohmann, G. Arctic Ocean sea ice cover during the penultimate glacial and the Last Interglacial. *Nat. Commun.* **8**, 373 (2017).
7. Kageyama, M. et al. A multi-model CMIP6-PMIP4 study of Arctic sea ice at 127 ka: sea ice data compilation and model differences. *Clim. Past* **17**, 37–62 (2021).
8. Nørgaard-Pedersen, N., Mikkelsen, N., Lassen, S. J., Kristoffersen, Y. & Sheldon, E. Reduced sea ice concentrations in the Arctic Ocean during the Last Interglacial period revealed by sediment cores off northern Greenland. *Paleoceanography* **22**, PA1218 (2007).
9. Guarino, M. V. et al. Sea-ice-free Arctic during the Last Interglacial supports fast future loss. *Nat. Clim. Change* **10**, 928–932 (2020).
10. Brigham-Grette, J. & Hopkins, D. Emergent marine record and paleoclimate of the Last Interglaciation along the Northwest Alaskan Coast. *Quat. Res.* **43**, 159–173 (1995).
11. Darling, K. F. et al. Genetic diversity and ecology of the planktonic foraminifers *Globigerina bulloides, Turborotalita quinqueloba* and *Neogloboquadrina pachyderma* off the Oman margin during the late SW monsoon. *Mar. Micropaleontol.* **137**, 64–77 (2017).
12. Greco, M., Werner, K., Zamelczyk, K., Rasmussen, T. L. & Kucera, M. Decadal trend of plankton community change and habitat shoaling in the Arctic gateway recorded by planktonic foraminifera. *Glob. Change Biol.* **28**, 1798–1808 (2022).
13. Anglada-Ortiz, G. et al. Planktic foraminiferal and pteropod contributions to carbon dynamics in the Arctic Ocean (north Svalbard margin). *Front. Mar. Sci.* **8**, 661158 (2021).
14. Ofstad, S. et al. Shell density of planktonic foraminifera and pteropod species *Limacina helicina* in the Barents Sea: relation to ontogeny and water chemistry. *PLoS ONE* **16**, e0249178 (2021).
15. Pados, T. & Spielhagen, R. F. Species distribution and depth habitat of recent planktic foraminifera in Fram Strait, Arctic Ocean. *Polar Res.* **33**, 22483 (2014).
16. Carstens, J., Hebbeln, D. & Wefer, G. Distribution of planktic foraminifera at the ice margin in the Arctic (Fram Strait). *Mar. Micropaleontol.* **29**, 257–269 (1997).
17. Volkmann, R. Planktic foraminifers in the outer Laptev Sea and the Fram Strait—Modern distribution and ecology. *J. Foraminifer. Res.* **30**, 157–176 (2000).
18. Carstens, J. & Wefer, G. Recent distribution of planktonic foraminifera in the Nansen Basin, Arctic Ocean. *Deep Sea Res. A* **39**, 507–524 (1992).
19. Rudels, B. et al. in *Arctic Climate Change* (eds Lemke, P. & Jacobi, H.-W.) 117–198 (Springer, 2012).
20. Bauch, H. A., Kandiano, E. S. & Helmke, J. P. Contrasting ocean changes between the subpolar and polar North Atlantic during the past 135 ka. *Geophys. Res. Lett.* **39**, L11604 (2012).
21. Alonso-Garcia, M., Sierro, F. J. & Flores, J. A. Arctic front shifts in the subpolar North Atlantic during the Mid-Pleistocene (800–400 ka) and their implications for ocean circulation. *Palaeogeogr. Palaeoclimatol. Palaeoecol.* **311**, 268–280 (2011).
22. Tesi, T. et al. Rapid Atlantification along the Fram Strait at the beginning of the 20th century. *Sci. Adv.* **7**, eabj2946 (2021).
23. Simstich, J., Sarnthein, M. & Erlenkeuser, H. Paired $\delta^{18}O$ signals of *Neogloboquadrina pachyderma* (s) and *Turborotalita quinqueloba* show thermal stratification structure in Nordic Seas. *Mar. Micropaleontol.* **48**, 107–125 (2003).
24. Jonkers, L., Brummer, G. J. A., Peeters, F. J. C., Van Aken, H. M. & De Jong, M. F. Seasonal stratification, shell flux, and oxygen isotope dynamics of leftcoiling *N. pachyderma* and *T. quinqueloba* in the western subpolar North Atlantic. *Paleoceanography* **25**, PA2204 (2010).
25. Nörgaard-Pedersen, N., Mikkelsen, N. & Kristoffersen, Y. The Last Interglacial warm period record of the Arctic Ocean: proxy-data support a major reduction of sea ice. *Mar. Geol.* **6**, 072002 (2009).
26. O'Regan, M. et al. Constraints on the Pleistocene chronology of sediments from the Lomonosov Ridge. *Paleoceanography* **23**, PA1S19 (2008).
27. O'Regan, M., Backman, J., Fornaciari, E., Jakobsson, M. & West, G. Calcareous nannofossils anchor chronologies for Arctic Ocean sediments back to 500 ka. *Geology* **48**, 1115–1119 (2020).
28. Jakobsson, M., Backman, J., Murray, A. & Løvlie, R. Optically stimulated luminescence dating supports central Arctic Ocean cm-scale sedimentation rates. *Geochem. Geophys. Geosyst.* **4**, 1016 (2003).
29. Vincent, W. F. & Mueller, D. Witnessing ice habitat collapse in the Arctic. *Science* **370**, 1031–1032 (2020).
30. Anderson, L. G. et al. Export of calcium carbonate corrosive waters from the East Siberian Sea. *Biogeosciences* **14**, 1811–1823 (2017).
31. Hald, M. & Steinsund, P. I. Benthic foraminifera and carbonate dissolution in the surface sediments of the Barents and Kara seas. *Ber. zur. Polarforsch.* **212**, 285–307 (1996).
32. Polyakov, I. V. et al. Greater role for Atlantic inflows on sea-ice loss in the Eurasian Basin of the Arctic Ocean. *Science* **356**, 285–291 (2017).
33. Lind, S., Ingvaldsen, R. B. & Furevik, T. Arctic warming hotspot in the northern Barents Sea linked to declining sea-ice import. *Nat. Clim. Change* **8**, 634–639 (2018).
34. Polyakov, I. V. et al. Weakening of cold halocline layer exposes sea ice to oceanic heat in the eastern Arctic Ocean. *J. Clim.* **33**, 8107–8123 (2020).
35. Pemberton, P. & Nilsson, J. The response of the central Arctic Ocean stratification to freshwater perturbations. *J. Geophyis. Res. Oceans* **121**, 792–817 (2016).
36. Schaefer, J. M. et al. Greenland was nearly ice-free for extended periods during the Pleistocene. *Nature* **540**, 252–255 (2016).
37. Christ, A. J. et al. A multimillion-year-old record of Greenland vegetation and glacial history preserved in sediment beneath 1.4 km of ice at Camp Century. *Proc. Natl Acad. Sci. USA* **118**, e2021442118 (2021).

38. Darling, K. F. & Wade, C. M. The genetic diversity of planktic foraminifera and the global distribution of ribosomal RNA genotypes. *Mar. Micropaleontol.* **67**, 216–238 (2008).
39. Helmens, K. F. et al. Prolonged interglacial warmth during the Last Glacial in northern Europe. *Boreas* **50**, 331–350 (2021).
40. Jackson, R. et al. Holocene polynya dynamics and their interaction with oceanic heat transport in northernmost Baffin Bay. *Sci. Rep.* **11**, 10095 (2021).
41. Belt, S. T. Source-specific biomarkers as proxies for Arctic and Antarctic sea ice. *Org. Geochem.* **125**, 277–298 (2018).
42. Belt, S. T. What do IP_{25} and related biomarkers really reveal about sea ice change? *Quat. Sci. Rev.* **204**, 216–219 (2019).
43. Malmierca-Vallet, I. et al. Simulating the Last Interglacial Greenland stable water isotope peak: the role of Arctic sea ice changes. *Quat. Sci. Rev.* **198**, 1–14 (2018).
44. Lunt, D. J. et al. Warm climates of the past—a lesson for the future? *Phil. Trans. R. Soc. A* **371**, 20130146 (2013).
45. Stroeve, J. C. et al. Trends in Arctic sea ice extent from CMIP5, CMIP3 and observations. *Geophys. Res. Lett.* **39**, L16502 (2012).
46. Stroeve, J., Holland, M. M., Meier, W., Scambos, T. & Serreze, M. Arctic sea ice decline: faster than forecast. *Geophys. Res. Lett.* **34**, L09501 (2007).
47. Dahl-Jensen, D. et al. Eemian Interglacial reconstructed from a Greenland folded ice core. *Nature* **493**, 489–494 (2013).
48. Hoffman, J. S., Clark, P. U., Parnell, A. C. & He, F. Regional and global sea-surface temperatures during the last interglaciation. *Science* **355**, 276–279 (2017).
49. Capron, E., Govin, A., Feng, R., Otto-Bliesner, B. L. & Wolff, E. W. Critical evaluation of climate syntheses to benchmark CMIP6/PMIP4 127 ka Last Interglacial simulations in the high-latitude regions. *Quat. Sci. Rev.* **168**, 137–150 (2017).
50. IPCC *Climate Change 2021: The Physical Science Basis* (eds Masson-Delmotte, V. et al.) (Cambridge Univ. Press, 2021).
51. Merz, N., Born, A., Raible, C. C. & Stocker, T. F. Warm Greenland during the Last Interglacial: the role of regional changes in sea ice cover. *Clim. Past* **12**, 2011–2031 (2016).
52. Muilwijk, M. et al. Divergence in Climate Model Projections of Future Arctic Atlantification. *J. Clim.* **36**, 1727–1748 (2023).
53. Jakobsson, M. et al. The International Bathymetric Chart of the Arctic Ocean Version 4.0. *Sci. Data* **7**, 176 (2020).
54. Fetterer, F., Knowles, K., Meier, W. N., Savoie, M. & Windnagel., A. K. *Sea Ice Index* Version 3 (NOAA, 2017); https://doi.org/10.7265/N5K072F8
55. Lisiecki, L. E. & Raymo, M. E. A Pliocene–Pleistocene stack of 57 globally distributed benthic $\delta^{18}O$ records. *Paleoceanography* **20**, PA1003 (2005).
56. Kucera, M. et al. Reconstruction of sea-surface temperatures from assemblages of planktonic foraminifera: multi-technique approach based on geographically constrained calibration data sets and its application to glacial Atlantic and Pacific Oceans. *Quat. Sci. Rev.* **24**, 951–998 (2005).
57. Husum, K. & Hald, M. Arctic planktic foraminiferal assemblages: Implications for subsurface temperature reconstructions. *Mar. Micropaleontol.* **96–97**, 38–47 (2012).
58. *Sea Ice and Snow Cover Extent* (NSIDC, 2021); https://www.ncdc.noaa.gov/snow-and-ice/extent/
59. Van Nieuwenhove, N. et al. Evidence for delayed poleward expansion of North Atlantic surface waters during the Last Interglacial (MIS5e). *Quat. Sci. Rev.* **30**, 934–946 (2011).
60. Zhuravleva, A., Bauch, H. A. & Van Nieuwenhove, N. Last Interglacial (MIS5e) hydrographic shifts linked to meltwater discharges from the East Greenland margin. *Quat. Sci. Rev.* **164**, 95–109 (2017).
61. Volkmann, R. *Planktic Foraminifer Ecology and Stable Isotope Geochemistry in the Arctic Ocean: Implications from Water Column and Sediment Surface Studies for Quantitative Reconstructions of Oceanic Parameters* (Alfred Wegener Institute for Polar and Marine Research, 2000).
62. Schauer, U. *The Expedition PS94 of the Research Vessel POLARSTERN to the Central Arctic Ocean in 2015* (AWI, 2016).
63. Fronval, T., Jansen, E., Haflidason, H. & Sejrup, H. P. Variability in surface and deep water conditions in the Nordic seas during the Last Interglacial period. *Quat. Sci. Rev.* **17**, 963–985 (1998).
64. Hanslik, D. *Late Quaternary Biostratigraphy and Paleoceanography of the Central Arctic Ocean*. PhD thesis, Stockholm Univ. (2011).
65. Irvalı, N. et al. Evidence for regional cooling, frontal advances, and East Greenland Ice Sheet changes during the demise of the Last Interglacial. *Quat. Sci. Rev.* **150**, 184–199 (2016).
66. Jakobsson, M. et al. Pleistocene stratigraphy and paleoenvironmental variation from Lomonosov Ridge sediments, central Arctic Ocean. *Glob. Planet Change* **31**, 1–22 (2001).
67. Mokeddem, Z. & McManus, J. F. Persistent climatic and oceanographic oscillations in the subpolar North Atlantic during the MIS6 glaciation and MIS5 interglacial. *Paleoceanography* **31**, 758–778 (2016).
68. Van Nieuwenhove, N. & Bauch, H. A. Last Interglacial (MIS5e) surface water conditions at the Vøring Plateau (Norwegian Sea), based on dinoflagellate cysts. *Polar Res.* **27**, 175–186 (2008).
69. Nørgaard-Pedersen, N., Mikkelsen, N. & Kristoffersen, Y. Arctic Ocean record of last two glacial–interglacial cycles off North Greenland/Ellesmere Island—implications for glacial history. *Mar. Geol.* **244**, 93–108 (2007).
70. Rasmussen, T. L., Thomsen, E., Kuijpers, A. & Wastegård, S. Late warming and early cooling of the sea surface in the Nordic seas during MIS5e (Eemian Interglacial). *Quat. Sci. Rev.* **22**, 809–821 (2003).

Methods

Core collection and core logging

Piston cores AO16-9PC and AO16-10PC were collected during the 2016 SWEDARCTIC expedition with icebreaker *Oden*[71]. While at sea, the bulk density, magnetic susceptibility and compressional wave velocity were measured at a 1 cm downcore resolution on whole cores using the Geotek Multi-Sensor Core. Measurements of X-ray fluorescence (XRF) were obtained with an ITRAX XRF core scanner at the Department of Geological Sciences, Stockholm University. The archive half of the core was scanned using a molybdenum tube set at 55 kV and 50 mA with a step size of 2 mm and an exposure time of 25 seconds. To remove background noise and produce analytically reliable counting statistics, the elemental data were normalized by zirconium, a conservative element commonly found in weathering-resistant minerals[72]. To optimize the original core photos, contrast, brightness and saturation were increased (Extended Data Fig. 6). This optimization changes dark brown to red colours and beige to yellow colours. Outliers from the multi-sensor core logger and XRF measurements, related to the edges of core sections (top and bottom), were removed.

Chronology and stratigraphy

The chronology (MIS1 to MIS6) of the new sediment cores AO16-10PC and AO16-9PC is derived through lithostratigraphic correlation to the well-dated sediment sequences found on the Lomonosov Ridge (Extended Data Fig. 6). Correlation is based on physical properties (bulk density, Mn/Zr variation) in combination with visual observations (for example, sediment colour). AO16-10PC and AO16-9PC were correlated to sediment core AO16-8GC and LRG12-7PC (Extended Data Fig. 6). This way, the stratigraphy of these cores could be fitted into the existing stratigraphic framework of the Lomonosov Ridge since core AO16-8GC was previously tied to LRG12-3PC[73]. LRG12-3PC is a key core because its chronology is constrained by nannofossil biostratigraphy[27]. In particular, the chronology of LRG12-3PC is anchored on the occurrence of two calcareous nannofossil taxa that have globally calibrated biozonations; *Pseudoemiliania lacunosa*, a species that went extinct during MIS12, and *Emiliania huxleyi*, a species that evolved during MIS8[74]. Importantly, the nannofossil biostratigraphy of LRG12-3PC provided evidence that strongly supported previously developed age models that were established for the classic drill core ACEX[26] and core 96/12-1pc[28] (Extended Data Fig. 6). Other than AO16-10PC and AO16-9PC, all presented cores within this study have age models that were developed in previous studies, and their corresponding references can be found in Extended Data Table 1. While the age model adopted here is based on the most widely accepted paradigm regarding the Arctic chronostratigraphy—that glacial/interglacial periods have distinct and generally readily identifiable facies (especially sediments predating MIS7)[73]—it should be acknowledged that alternative age models based on Uranium decay series have been proposed[75]. These alternative age models would attribute the *T. quinqueloba* peaks to interglacials between MIS7 and MIS13[76–78]. From a climatological perspective, MIS5e is the most logical candidate for a seasonally ice-free Arctic Ocean as it is considered the most intense interglacial of the past 800 kyr, closely followed by MIS11c[79]. MIS7 is an interglacial of intermediate intensity, and MIS9 is considered fairly intense[79]. MIS13 is one of the weakest interglacials in the past 800 kyr (ref. 79). Therefore, even if our evidence for a seasonally ice-free ocean would be later attributed to an older (colder) interglacial, this would strongly imply that MIS5e would have been seasonally ice free as well.

Microfossil analysis

In sediment cores AO16-10PC, AO16-9PC, LRG12-3PC and AO16-8GC, samples of 1 cm thickness (5 cm^3) were obtained throughout the respective MIS5 intervals. In addition, a series of 2-cm-thick samples that were used for an initial general assessment of microfossil content were also analysed. The samples were sieved over a 63-µm-mesh sieve, dried in an oven (<40 °C), weighed and transferred to glass vials. Counting of planktic foraminifera was performed on the dried >63 µm fraction. For core 96/12-1pc, pre-existing samples (63–125 µm) were analysed. Analysis of the >63 µm fraction is important because Arctic populations of some species (such as *T. quinqueloba*) are small and might be absent in larger size fractions[57,80]. Representative samples containing at least 300 tests were obtained by sediment splitting, performed using a microsplitter (ASC Scientific MS-1). Counting and identification of foraminifers was performed using a Leica M205C microscope. The census work is based on the taxonomic framework of ref. 12, which recognizes a single species name for *N. pachyderma* and *T. quinqueloba*, without distinguishing constituent morphotypes[81]. Special attention was given to avoid counting the lightly calcified Nps-5 *N. pachyderma* morphotype as *T. quinqueloba*[82–84]. Our taxonomy was cross-checked and verified using scanning electron microscopy to study the wall textures (Extended Data Fig. 9). Scanning electron microscope (SEM) imaging was carried out using a JSM-7000 F SEM for *T. quinqueloba* (accelerating voltage = 10 kV, working distance = 9.9 mm) and a TM 3000 for *N. pachyderma*. Both SEMs are housed in the Department of Materials and Environmental Chemistry, Stockholm University. The specimens were mounted on sticky carbon discs and gold coated before analysis (2 × 60 seconds, applied current of 20 mA). We found no evidence for carbonate dissolution within the MIS5e interval, and since the thin-shelled *T. quinqueloba* is more prone to dissolution than *N. pachyderma*[14], the interpretations would remain the same even if differential dissolution had been at play.

Different morphotypes of *N. pachyderma* were observed but grouped into the same category. Benthic foraminifera contained a very small percentage of the total foraminifera abundance (<1% of the planktic plus benthic population). The most common benthic foraminifers include *Oridorsalis tener, Bolivina arctica, Epistominella arctica, Stetsonia horvathi* and *Cibicides wuellerstorfi*. A literature review was performed to document previously reported *T. quinqueloba* occurrences in the Arctic and Northern Atlantic oceans; these sampling sites and their respective references are found in Extended Data Table 1.

We also examined the cores LRG12-7PC, AO16-8GC and LRG12-3PC in terms of recording the first appearance of the key species *E. huxleyi*. A 10 cm sampling was carried out on the top 1.0–1.5 m of each core. In some cases, the sampling resolution was increased to 5, 3 and 2 cm in dark-coloured units and intervals close to biozonal boundaries. Smear slides were prepared from unprocessed sediments and were examined under a polarizing light microscope (Zeiss Axio Scope.A1) at ×1,000 and ×1,250 magnifications.

Data availability

All related data will be made available on the Bolin Centre database (https://bolin.su.se/data/oden-ao-2016-sediment-9pc-10pc-physprop-1 and http://bolin.su/se/data/vermassen-2023-foraminifera-1) upon publication. Source data are provided with this paper.

References

71. Gårdfeldt, K. & Lindgren, Å. *SWEDARCTIC Arctic Ocean 2016* (Swedish Polar Reseaech Secretariat, 2016); http://www.diva-portal.org/smash/get/diva2:1081650/FULLTEXT01.pdf
72. Rothwell, R. G. & Croudace, I. w. in *Micro-XRF Studies of Sediment Cores: Applications of a Non-destructive Tool for the Environmental Sciences* (eds Croudace, I. W. & Rothwell, R. G.) 25–102 (Springer, 2015); https://doi.org/10.1007/978-94-017-9849-5_2
73. Vermassen, F., O'Regan, M., West, G., Cronin, T. M. & Coxall, H. K. Testing the stratigraphic consistency of Pleistocene microfossil bioevents identified on the Alpha and Lomonosov ridges, Arctic Ocean. *Arct. Antarct. Alp. Res.* **53**, 309–323 (2021).

74. Thierstein, H. R., Geitzenauer, K. R., Molfino, B. & Shackleton, N. J. Global synchroneity of late Quaternary coccolith datum levels validation by oxygen isotopes. *Geology* **5**, 400–404 (1977).
75. Hillaire-Marcel, C. et al. A new chronology of late Quaternary sequences from the central Arctic Ocean based on 'extinction ages' of their excesses in ^{231}Pa and ^{230}Th. *Geochem. Geophys. Geosyst.* **18**, 4573–4585 (2017).
76. Hillaire-Marcel, C. & de Vernal, A. A comment about 'A sedimentary record from the Makarov Basin, Arctic Ocean, reveals changing Middle to Late Pleistocene glaciation patterns'. *Quat. Sci. Rev.* **270**, 107176 (2021).
77. Purcell, K., Hillaire-Marcel, C., de Vernal, A., Ghaleb, B. & Stein, R. Potential and limitation of ^{230}Th-excess as a chronostratigraphic tool for late Quaternary Arctic Ocean sediment studies: an example from the southern Lomonosov Ridge. *Mar. Geol.* **448**, 106802 (2022).
78. W. Xiao, *et al*. *Quat. Sci. Rev*. 279, 107239 (2022).
79. Past Interglacials Working Group of PAGES Interglacials of the last 800,000 years. *Rev. Geophys.* **54**, 162–219 (2016).
80. O'Regan, M. et al. Stratigraphic occurrences of sub-polar planktic foraminifera in Pleistocene sediments on the Lomonosov Ridge, Arctic Ocean. *Front. Earth Sci.* https://doi.org/10.3389/feart.2019.00071 (2019).
81. Brummer, G.-J. A. & Kučera, M. Taxonomic review of living planktonic foraminifera. *J. Micropalaeontol.* **41**, 29–74 (2022).
82. El Bani Altuna, N., Pieńkowski, A. J., Eynaud, F. & Thiessen, R. The morphotypes of *Neogloboquadrina pachyderma*: isotopic signature and distribution patterns in the Canadian Arctic Archipelago and adjacent regions. *Mar. Micropaleontol.* **142**, 13–24 (2018).
83. Eynaud, F. et al. Morphological variability of the planktonic foraminifer *Neogloboquadrina pachyderma* from ACEX cores: implications for Late Pleistocene circulation in the Arctic Ocean. *Micropaleontology* **55**, 101–116 (2009).
84. Adler, R. E. et al. Sediment record from the western Arctic Ocean with an improved late Quaternary age resolution: HOTRAX core HLY0503-8JPC, Mendeleev Ridge. *Glob. Planet. Change* **68**, 18–29 (2009).
85. Schlitzer, R. Data analysis and visualization with Ocean Data View. *CMOS Bull. SCMO* **43**, 9–13 (2015).
86. Boyer, T. P. et al. *World Ocean Atlas 2018* (NOAA, 2018).

Acknowledgements

The crew and captains of IB *Oden* are thanked for core collection during the multiple expeditions that have been conducted over the past 20 years. C. Johansson is thanked for XRF scanning. K. Jansson is thanked for help with SEM imaging. F.V., M.O. and A.d.B. were supported by the Swedish Research Council under Grants DNR 2019-03757, DNR 2020-04379 and DNR 2020-04791, respectively. T.M.C. was funded by the US Geological Survey Climate Research and Development Program. Any use of trade, firm or product names is for descriptive purposes only and does not imply endorsement by the US government.

Author contributions

F.V. conducted foraminifera analysis, carried out data analysis and wrote the study with contributions from all authors. F.V., H.K.C. and M.O. conceptualized the study. F.V., H.K.C., M.O. and A.d.B. performed data interpretation. M.R. performed nannofossil analysis. F.S, G.W., M.R, T.M.C. and M.J. reviewed the paper and provided edits. All authors reviewed and contributed to the paper.

Funding

Open access funding provided by Stockholm University.

Competing interests

The authors declare no competing interests.

Additional information

Extended data is available for this paper at https://doi.org/10.1038/s41561-023-01227-x.

Supplementary information The online version contains supplementary material available at https://doi.org/10.1038/s41561-023-01227-x.

Correspondence and requests for materials should be addressed to Flor Vermassen.

Peer review information *Nature Geoscience* thanks Mohamed Ezat, Maciej Telesiński and for their contribution to the peer review of this work. Primary Handling Editor: James Super, in collaboration with the *Nature Geoscience* team.

https://doi.org/10.1038/s41561-023-01227-x

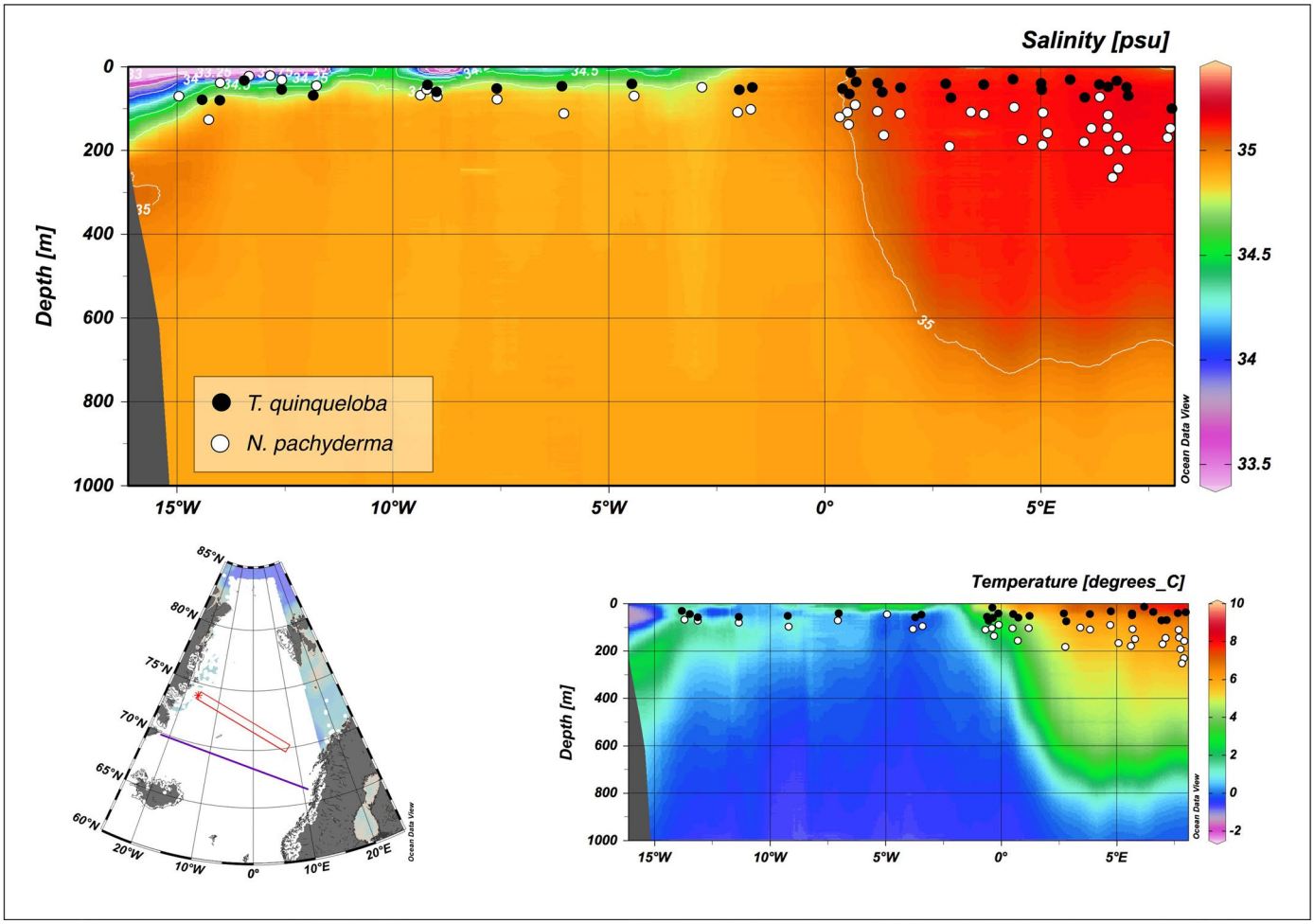

Extended Data Fig. 1 | Apparent calcification depths of *Neogloboquadrina pachyderma* and *Turborotalita quinqueloba* from a transect of sediment surface samples in the Northern North Atlantic (purple line in the inset map). Calcification depths[23] are projected onto the modelled salinities (upper panel) and temperatures (lower right panel) of a nearby transect (red box in the inset map) from ref. 85. Figure created with Ocean Data View[85].

https://doi.org/10.1038/s41561-023-01227-x

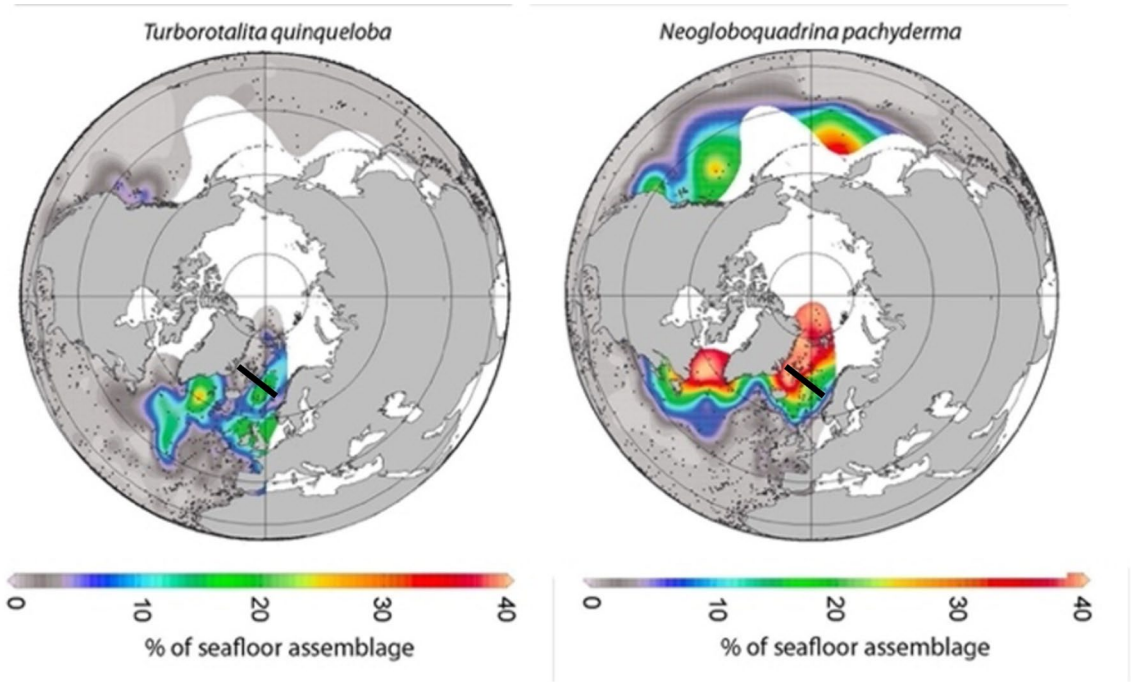

Extended Data Fig. 2 | Distribution of *N. pachyderma* and *T. quinqueloba* in high northern latitude surface sediments. Black line indicates the position of the oceanographic profile in Fig. ED1. Figure adapted with permission from ref. 80 under a Creative Commons license CC BY 4.0. Gridded distributions produced using the database from ref. 56. Figure created with Ocean Data View.

https://doi.org/10.1038/s41561-023-01227-x

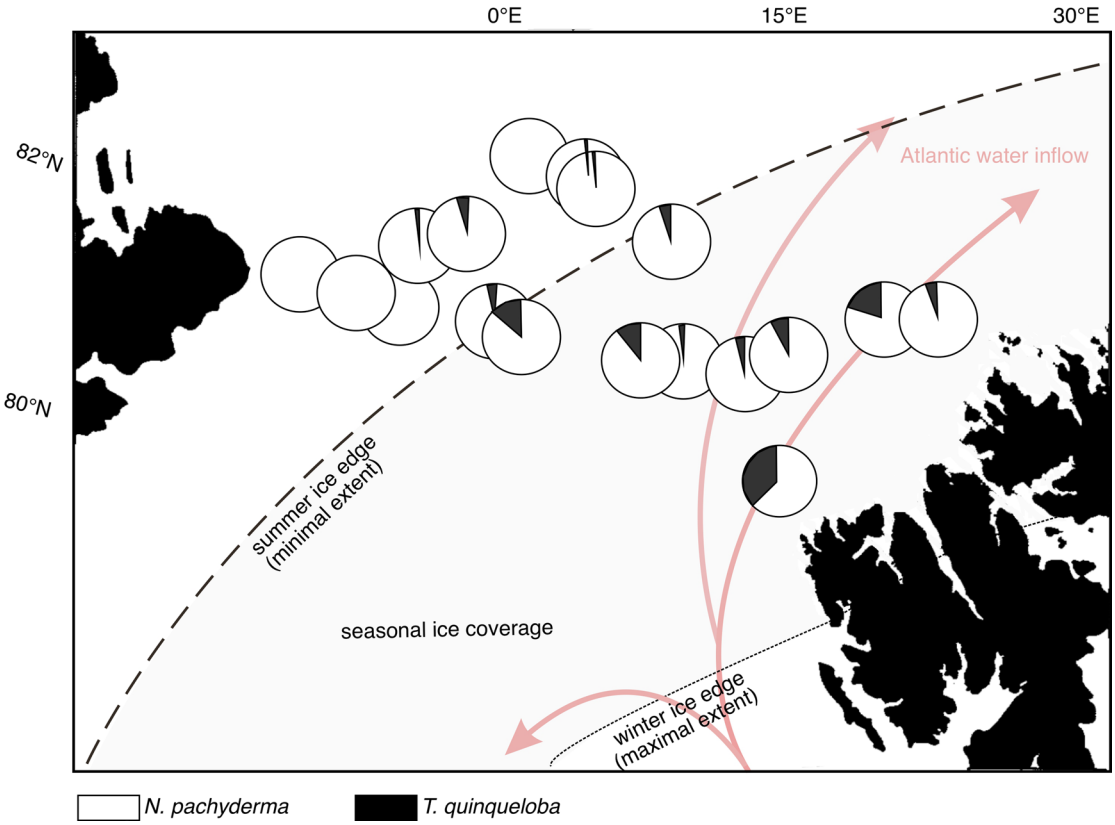

Extended Data Fig. 3 | Relative abundance of *N. pachyderma* and *T. quinqueloba* in surface sediments (pie charts) in the Fram Strait. Ice cover and Atlantic Water inflow are also indicated. Figure adapted with permission from ref. 61, Alfred Wegener Institute.

https://doi.org/10.1038/s41561-023-01227-x

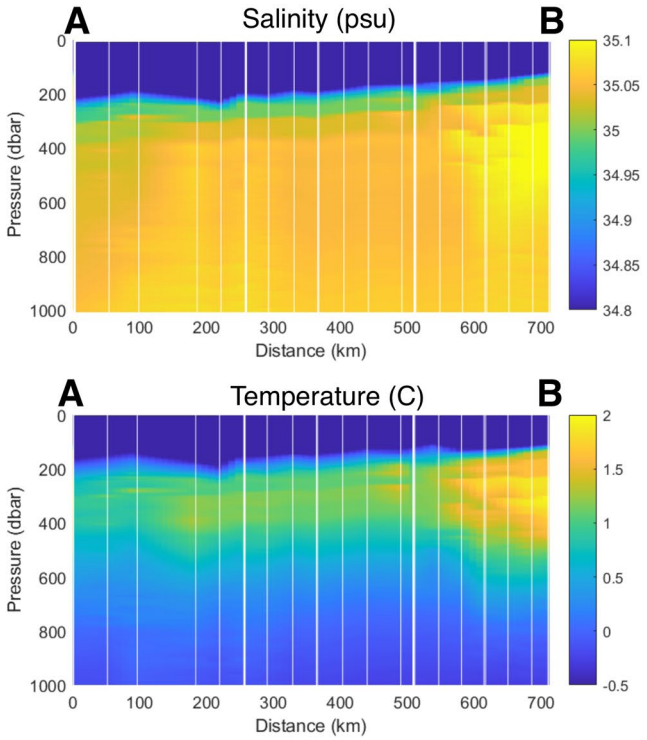

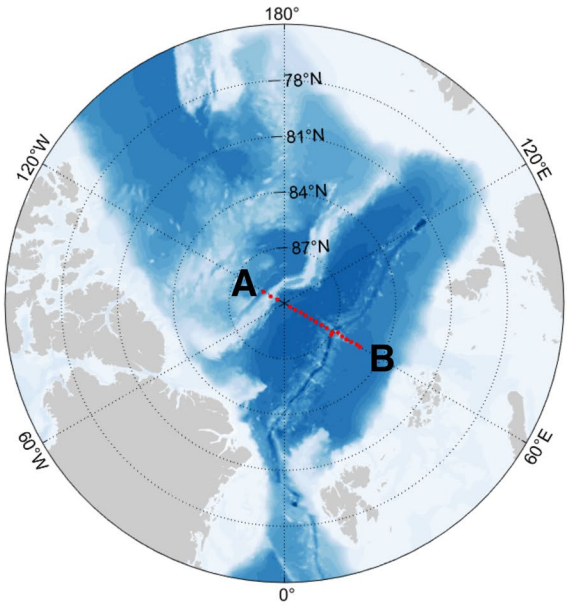

Extended Data Fig. 4 | Salinity and temperature profile along the Nansen basin obtained during the PS94 cruise in 2015 with RV Polarstern. Vertical white lines mark the positions of the CTD profiles. The profiles illustrate the typical stratification that is generally present in the modern central Arctic Ocean[62]. Atlantic-derived waters flowing at water depths 200–500m underlie a cold, ca. 200m thick, low salinity water mass. The core of Atlantic Water inflow can be observed along the Siberian side of the Arctic Ocean.

https://doi.org/10.1038/s41561-023-01227-x

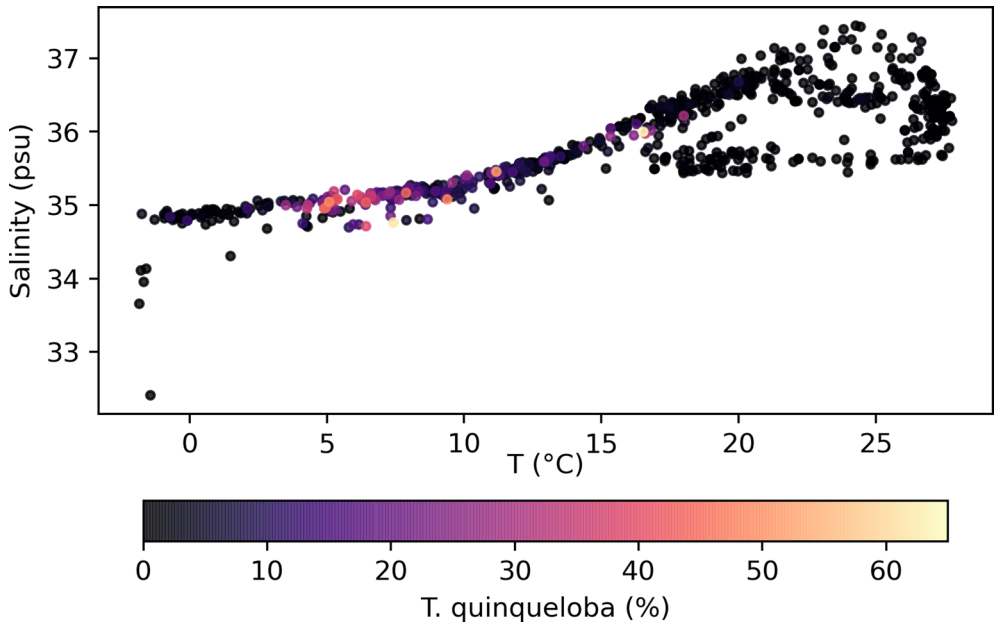

Extended Data Fig. 5 | Abundances of *T. quinqueloba* found in surface sediments, colour coded according to abundance, plotted in the temperature-salinity space. The data for abundances in seafloor sediments are from the Kucera[56] dataset and supplemented with data from this study. The temperature and salinity values are from 50 m water depth and were obtained from the world ocean atlas database and represent median annual values for the period 1981–2010[86].

https://doi.org/10.1038/s41561-023-01227-x

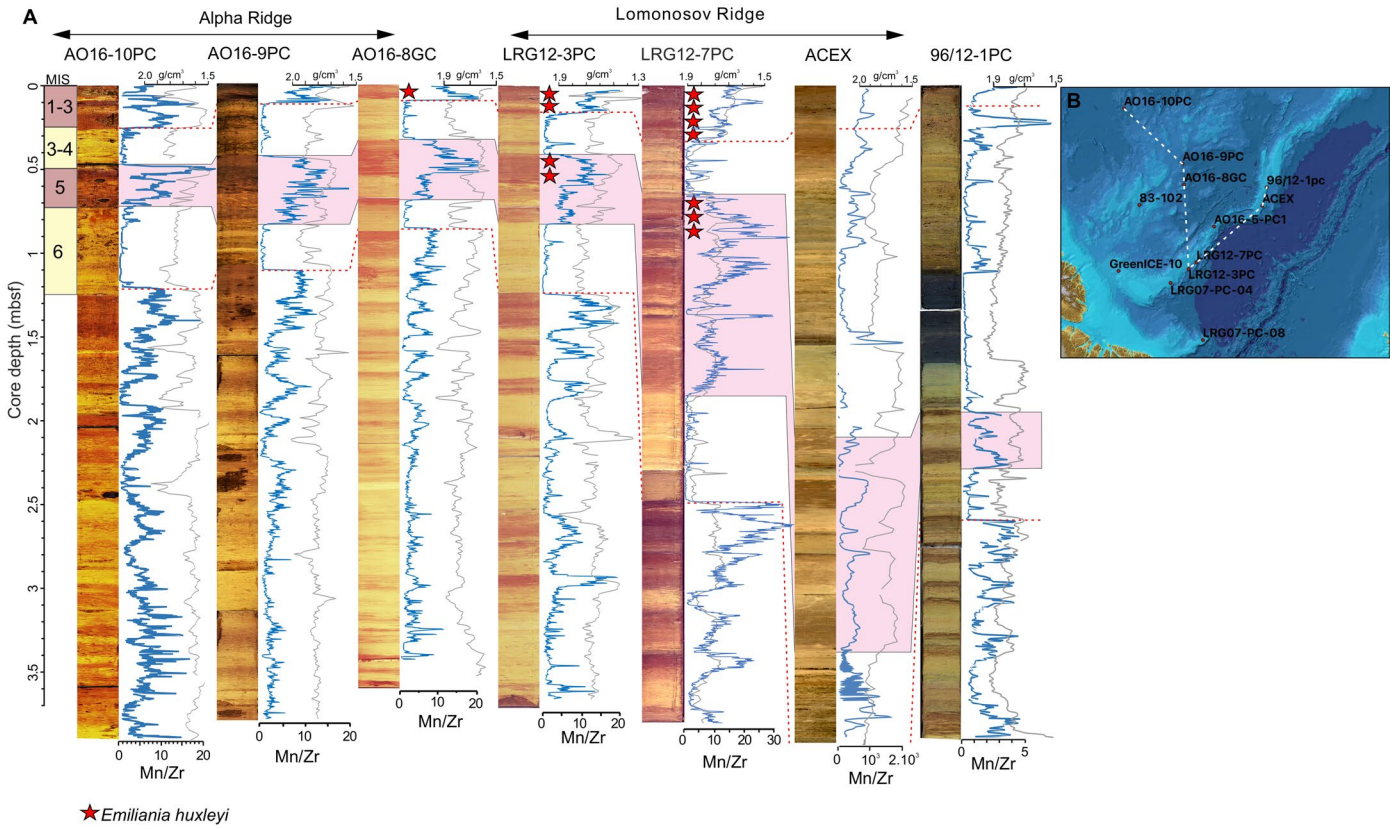

Extended Data Fig. 6 | Stratigraphic correlation between sediment cores presented in this study. a) Core images, together with Mn(/Zr) profiles and bulk density measurements. Note that bulk density scales are flipped. MIS stages are indicated on the left, the interval with red shading indicates the MIS 5 interval. **b**) Map illustrating core positions, with yellow line indicating the transect. **c**) Full core images of the presented cores, dotted line indicates the sections of the cores presented in A. Panel B adapted from ref. 53 under a Creative Commons license CC BY 4.0.

https://doi.org/10.1038/s41561-023-01227-x

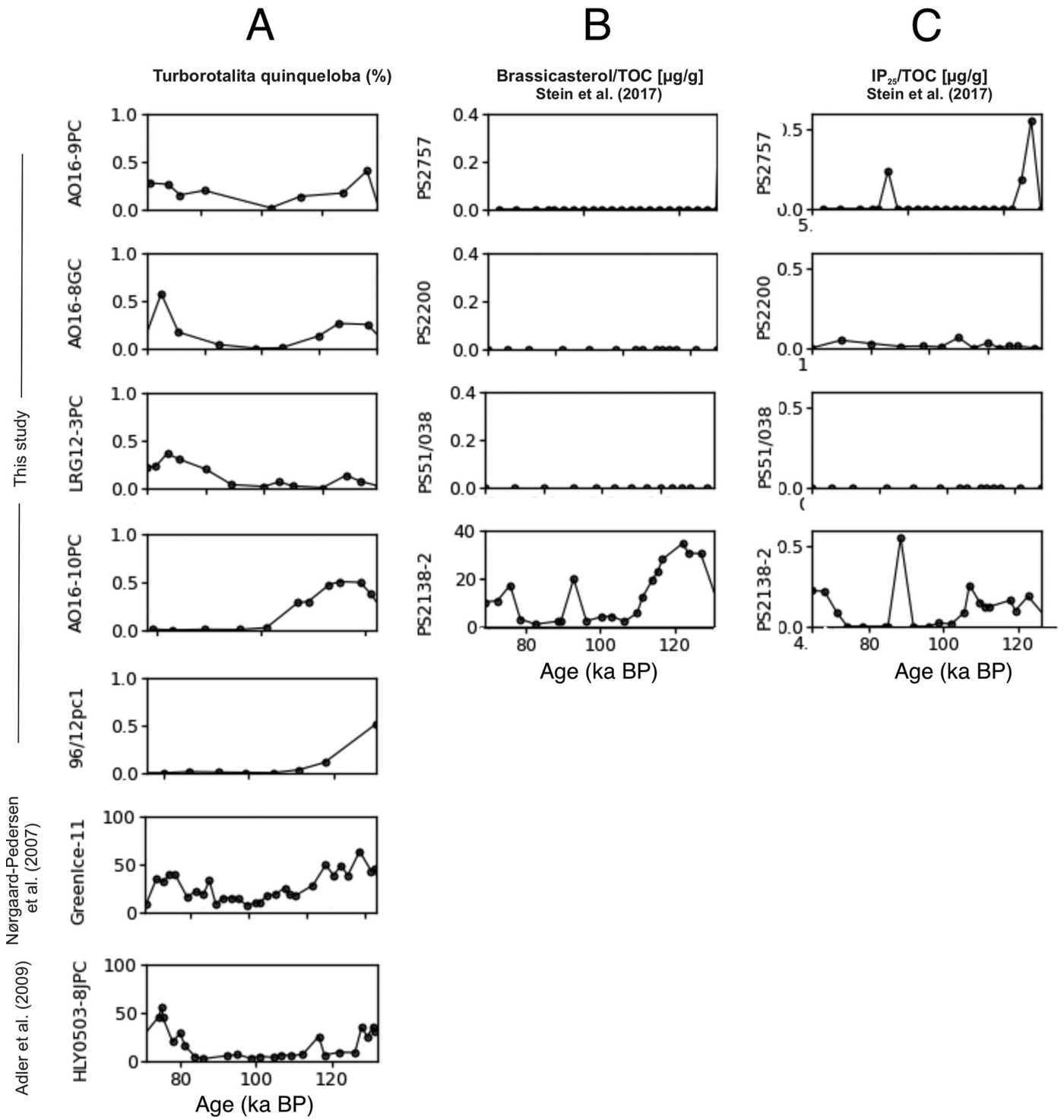

Extended Data Fig. 7 | Comparison of proxy data used to reconstruct sea-ice conditions during MIS 5 in the (central) Arctic Ocean. a) Abundance plots of the sub-polar planktonic foraminifer *T. quinqueloba*. **b**) Concentrations of the biomolecule brassicasterol, an indicator of open waters[6]. **c**) Concentrations of the biomolecule. IP_{25}, an indicator of seasonal sea-ice[6]. The data is plotted according to age and with indications of MIS 5 substages.

https://doi.org/10.1038/s41561-023-01227-x

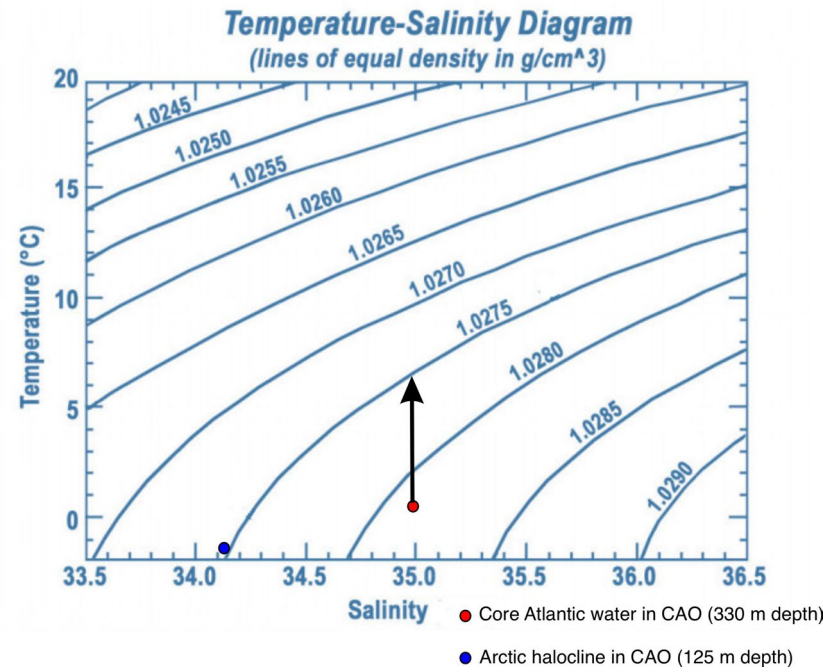

Extended Data Fig. 8 | *Properties of the Atlantic Water and halocline as recorded in the modern Arctic ocean, plotted in the temperature-salinity space.* The arrow indicates that an increase of the Atlantic Water layer to 6–7 °C would result in reaching the same density as the halocline, allowing mixing of both water masses. This provides a possible mechanism to explain shallowing/erosion of the halocline during the LIG.

https://doi.org/10.1038/s41561-023-01227-x

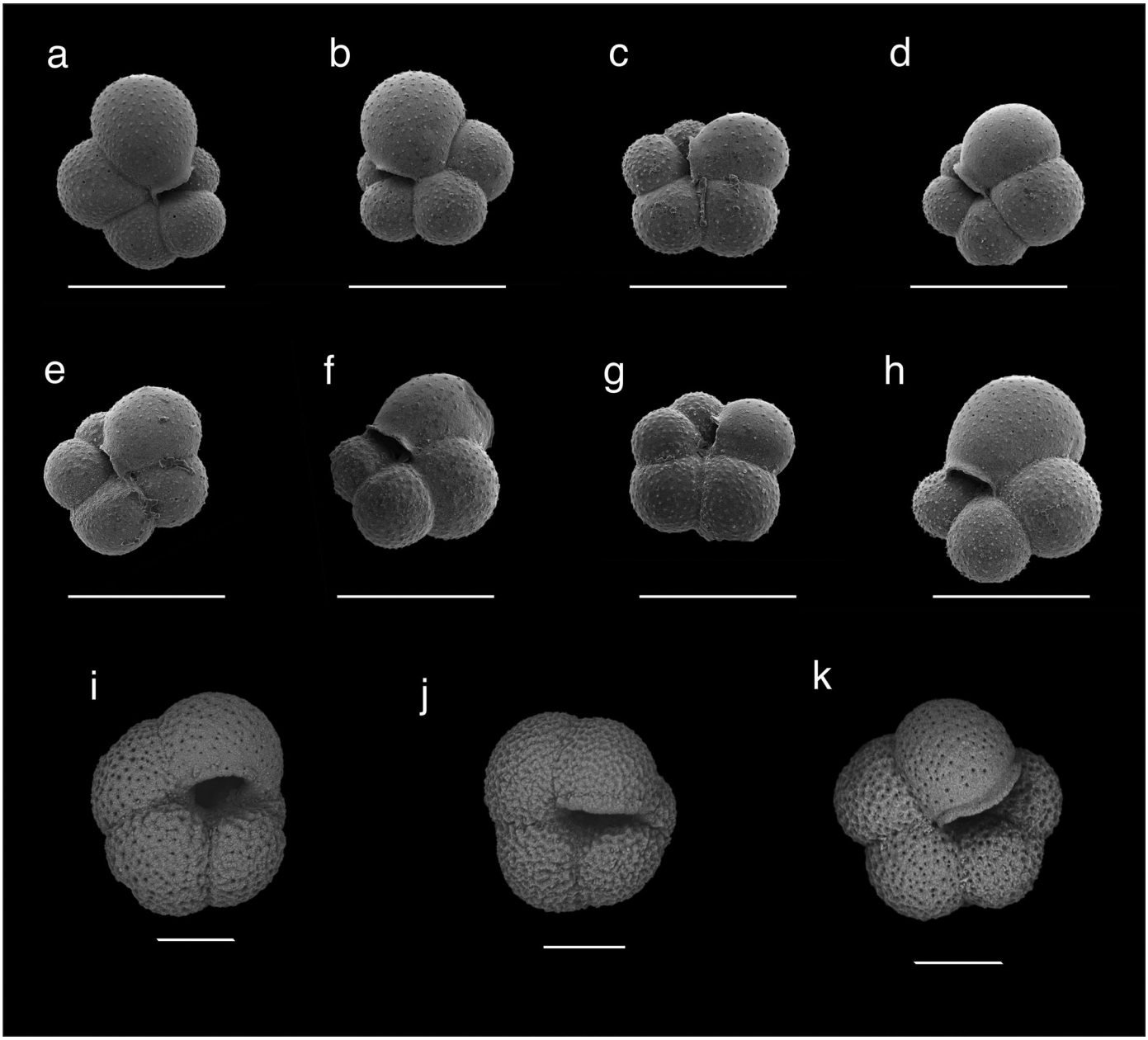

Extended Data Fig. 9 | SEM images showing morphological variability of planktonic foraminifers found in AO16-8GC. a) to **h**): *T. quinqueloba* (0.31–0.33 mbsf). (i) to (k): *N. pachyderma*. **i**) and **j**): 0.10–12 mbsf, **k**): 1.09–1.11 mbsf. The scale bar is 100 micron.

https://doi.org/10.1038/s41561-023-01227-x

Extended Data Table. 1 | Compilation of study sites with *T. quinqueloba* during MIS 5e in the northern North-Atlantic and Arctic Ocean

Core	Lat	Lon	Water depth (m)	Reference
M23351	70.35	18.22	1673	Zhuravleva et al., 2017
M23352	70.00	-12.43	1819	Van Nieuwenhove et al., 2013
M23071-3	67.08	2.9	1306	Van Nieuwenhove et al., 2008
ODP907A	69.24982	-12.69823	1800	Jansen et al., 2000
M23323-1	67°46N	5°55E	1286	Van Nieuwenhove et al., 2011
M23455-3	76°51N	8°22E	2497	Van Nieuwenhove et al., 2011
MD03-2664	57°26N	48°36W	3440	Irvali et al., 2016
HM57-7	68°26N	04°34E	1620	Fronval et al., 1998
HM71-19	69°29N	9°31W	2210	Fronval et al., 1998
HM79-31	67°02N	7°57W	1790	Fronval et al., 1998
HM71-25	67°59N	0°14E	2855	Fronval et al., 1998
ODP644	66°40N	4°34E	1227	Fronval et al., 1998
AO16-8-GC	86.7795	-140.6433	2620	Vermassen et al., 2021
AO16-9PC	85.9557	-148.3258	2212	This study
AO16-10PC	82.398	-141.245	2872	This study
LRG07-PC04	86.70117	-53.76717	811	Hanslik (thesis)
LRG07-PC08	85.31983	-14.8575	1038	Hanslik (thesis)
LRG12-7PC	88.19764	-55.68453	2522	O'Regan et al., 2019
AO16-5PC	89.078	-130.547	1253	O'Regan et al., 2019
LRG12-3PC	87.72472	-54.42528	1607	O'Regan et al., 2020
GreenICE-10	84.8	-74.283333	1040	Nørgaard-pedersen et al., 2007
96/12-1pc	87°05'51N	144°46'22E	1003	Jakobsson et al., 2001
HLY0503-8JPC	79°35.6'N	172°30.1'W	2792	Adler et al., 2009
ARC7-E25	78.573	179.261	1200	Zhao et al., 2022